Hindawi
Advances in Condensed Matter Physics
Volume 2019, Article ID 1539865, 11 pages
https://doi.org/10.1155/2019/1539865

Research Article

Waveguide Propagation of Light in Polymer Porous Films Filled with Nematic Liquid Crystals

A. D. Kiselev,[1] S. V. Pasechnik,[2] D. V. Shmeliova,[2] A. P. Chopik,[2] D. A. Semerenko,[2] and A. V. Dubtsov[2]

[1]*Saint Petersburg National Research University of Information Technologies, Mechanics and Optics (ITMO University), Kronverkskiy Prospekt 49, 197101 Saint Petersburg, Russia*
[2]*MIREA - Russian Technological University, Vernadskogo Ave., 78, Moscow 119454, Russia*

Correspondence should be addressed to D. V. Shmeliova; shmeliova@mail.ru

Received 5 October 2018; Accepted 13 January 2019; Published 13 February 2019

Academic Editor: Charles Rosenblatt

We theoretically analyze the waveguide regime of light propagation in a cylindrical pore of a polymer matrix filled with liquid crystals assuming that the effective radial optical anisotropy is biaxial. From numerical analysis of the dispersion relations, the waveguide modes are found to be sensitive to the field-induced changes of the anisotropy. The electrooptic properties of the polymer porous polyethylene terephthalate (PET) films filled with the nematic liquid crystal 5CB are studied experimentally and the experimental results are compared with the results of the theoretical investigation.

1. Introduction

Liquid crystals (LCs) are known to be of primary importance in the modern display industry. A unique combination of physical properties of LCs provides a means to control light propagation through micron-sized LC layers using electric fields at low operating voltages and small energy consumption. The key feature of liquid crystal materials that underlies excellent electrooptical characteristics of LCs and makes them promising for photonic applications is the high sensitivity of LC orientational structures to both external fields and conditions at bounding surfaces. In particular, the use of LC in microstructured waveguides [1, 2] and waveguides based on photonic crystals [3, 4] is mainly determined by this feature providing an efficient tool to adjust optical characteristics of waveguide photonic devices by means of the external (electric) field.

Utilization of LCs in nondisplay applications such as photonic devices [5] and a variety of sensors [6, 7] faces a number of challenges. These include a slow response time of orientational transformations for the devices of THz photonics based on thick layers of LC [8], high operating voltages needed to tune propagation of light in photonics fibers filled with LC [9], and relatively low sensitivity of planar LC layers to impurities in biosensensing applications [7]. Some of these problems can be solved by usage of composite materials, like PDLC, LC emulsions, and porous films filled with LC.

In this paper the electrooptical properties of the porous polymer films filled with nematic liquid crystals will be our primary concern. Recently such type of composite material—the polymer polyethylene terephthalate (PET) film—with normally oriented open pores of submicron and micron sizes, filled with LC, was experimentally studied in [10, 11]. It was shown that such systems are very promising for applications in photonic waveguide and terahertz (THz) devices [11, 12].

In particular, we have observed pronounced changes of light intensity transmitted through the film induced by applying low frequency ac electric field. Similarly, modulation of the light intensity can also be caused by heating of the sample via absorption of blue light by the azo-dye layer adsorbed on the internal surfaces of the pores. The hypothesis put forward in [11] to explain the experimental results assumes that breaking of the waveguide regime of light propagation is responsible for the light modulation.

These results motivate theoretical considerations of this paper that aimed to examine the waveguide regime of light propagation in cylindrical LC pores. In our calculations, we shall treat the LC material as an effective medium with variable anisotropy embedded in an isotropic environment. Though similar approach was previously used in [2], it was not applied to analyze the waveguide regime. Rigorous analysis of the problem based on numerical solution of Maxwell's equations [13] showed that waveguide propagation of light in a cylindrical cavity surrounded by isotropic media is crucially influenced by the orientational structure formed inside the pore [14–16]. On the other hand, the type of the orientational configuration is governed by a number of parameters such as the Frank elastic constants, the surface anchoring strengths and orientation of the easy axes, and the diameter of LC pores [17–21]. The paper is organized as follows.

In Section 2 we present the details of our theoretical analysis and systematically study the effects of effective LC anisotropy on the waveguide regime of light propagation. In Section 3, we describe the experimental results obtained for the porous PET films with micron and submicron pores filled with LC 5CB. In our discussion of these results we, in particular, demonstrate a qualitative agreement between the experimental data and the theoretical predictions. Concluding remarks are given in Section 4.

2. Theory

2.1. Basic Equations. We begin with the Maxwell equations for a monochromatic electromagnetic wave

$$\begin{aligned} \nabla \times \mathbf{E} &= ik_0\mu\mathbf{H}, \\ \nabla \times \mathbf{H} &= -ik_0\mathbf{D}, \quad \mathbf{D} = \boldsymbol{\epsilon}\mathbf{E}, \end{aligned} \tag{1}$$

where $k_0 = \omega/c$ is the free space wavenumber and $\boldsymbol{\epsilon}$ is the dielectric tensor, which propagate along the axis of a cylindrical waveguide (the z axis). Assuming that the electromagnetic field can be written in the factorized form $\{\mathbf{E}, \mathbf{H}\}e^{i(k_z z-\omega t)}$, we shall use the cylindrical coordinate system $\{\rho, \phi, z\}$ and separate out the longitudinal and transverse parts of both the electromagnetic field and the gradient operator as follows:

$$\begin{aligned} \mathbf{E} &= \mathbf{E}_T + E_z\hat{\mathbf{z}}, \\ \nabla &= \nabla_T + \hat{\mathbf{z}}\partial_z = \nabla_T + ik_z\hat{\mathbf{z}}, \end{aligned} \tag{2}$$

$$\nabla_T = \hat{\mathbf{x}}\partial_x + \hat{\mathbf{y}}\partial_y = \hat{\mathbf{e}}_\rho\partial_\rho + \hat{\mathbf{e}}_\phi\rho^{-1}\partial_\phi, \tag{3}$$

where $\hat{\mathbf{e}}_\rho = \cos\phi\hat{\mathbf{x}} + \sin\phi\hat{\mathbf{y}}$ and $\hat{\mathbf{e}}_\phi = -\sin\phi\hat{\mathbf{x}} + \cos\phi\hat{\mathbf{y}}$. With the help of the relation $\hat{\mathbf{z}} \times (\nabla \times \mathbf{E}) = \nabla_T E_z - ik_z\mathbf{E}_T$, we obtain the transverse part of Maxwell's equations (1) in the following form:

$$\begin{aligned} \nabla_T E_z - ik_z\mathbf{E}_T &= ik_0\mu\hat{\mathbf{z}} \times \mathbf{H}_T, \\ \left(\hat{\mathbf{z}} \times \nabla_T\right) H_z - ik_z\hat{\mathbf{z}} \times \mathbf{H}_T &= ik_0\mathbf{D}_T. \end{aligned} \tag{4}$$

In what follows, we, following the results of the paper [2], restrict ourselves to the case of effective radial biaxial anisotropy characterized by the constitutive relations of the following form:

$$\mathbf{D}_T = \boldsymbol{\epsilon}_T\mathbf{E}_T = \begin{pmatrix} \epsilon_\rho & 0 \\ 0 & \epsilon_\phi \end{pmatrix}\begin{pmatrix} E_\rho \\ E_\phi \end{pmatrix}, \quad D_z = \epsilon_{zz}E_z. \tag{5}$$

Note that the case of radial anisotropy was also considered in the theory of light scattering by optically anisotropic cylindrical particles developed in [22, 23].

From equations (4) it is not difficult to express the transverse components of the electromagnetic field $\{\mathbf{E}_T, \mathbf{H}_T\}$, in terms of the longitudinal components $\{E_z, H_z\}$, as follows:

$$i\left(k_z^2 - k_0^2\mu\boldsymbol{\epsilon}_T\right)\mathbf{E}_T = k_z\nabla_T E_z - k_0\mu\left(\hat{\mathbf{z}} \times \nabla_T\right)H_z, \tag{6}$$

$$i\left(k_z^2 - k_0^2\mu\boldsymbol{\epsilon}_T\right)\hat{\mathbf{z}} \times \mathbf{H}_T = k_z\left(\hat{\mathbf{z}} \times \nabla_T\right)H_z - k_0\boldsymbol{\epsilon}_T\nabla_T E_z. \tag{7}$$

For convenience, we shall introduce the dimensionless parameters

$$\begin{aligned} r &= k_0\rho, \\ q_z &= \frac{k_z}{k_0}, \\ q_\rho^2 &= \mu\epsilon_\rho - q_z^2 = n_\rho^2 - q_z^2, \\ q_\phi^2 &= \mu\epsilon_\phi - q_z^2 = n_\phi^2 - q_z^2 \end{aligned} \tag{8}$$

and write down the expressions for the transverse components in the explicit form:

$$E_\rho = \frac{i}{q_\rho^2 r}\left\{q_z r\partial_r E_z + \mu\partial_\phi H_z\right\}, \tag{9}$$

$$E_\phi = \frac{i}{q_\phi^2 r}\left\{q_z\partial_\phi E_z - \mu r\partial_r H_z\right\}, \tag{10}$$

$$H_\rho = \frac{i}{q_\phi^2 r}\left\{q_z r\partial_r H_z - \epsilon_\phi\partial_\phi E_z\right\}, \tag{11}$$

$$H_\phi = \frac{i}{q_\rho^2 r}\left\{q_z\partial_\phi H_z + \epsilon_\rho r\partial_r E_z\right\}. \tag{12}$$

Equations for the longitudinal components can be obtained using the divergence relations: $(\nabla \cdot \mathbf{D}) = (\nabla \cdot \mathbf{H}) = 0$ (these follow from Maxwell's equations (1)), which can be conveniently recast into the following form:

$$\begin{aligned} \left(\nabla_T \cdot \mathbf{D}_T\right) &= -ik_z D_z, \\ \left(\nabla_T \cdot \mathbf{H}_T\right) &= \left(\hat{\mathbf{z}} \times \nabla_T \cdot \hat{\mathbf{z}} \times \mathbf{H}_T\right) = -ik_z H_z. \end{aligned} \tag{13}$$

After eliminating the transverse components from the relations (6)–(7) with the help of Eq. (13), we have

$$\left\{\nabla_T \boldsymbol{\epsilon}_T \left[k_z^2 - k_0^2 \mu \boldsymbol{\epsilon}_T\right]^{-1} \nabla_T - \epsilon_{zz}\right\} E_z = q_z \nabla_T \left[k_z^2 - k_0^2 \mu \boldsymbol{\epsilon}_T\right]^{-1} (\hat{\mathbf{z}} \times \nabla_T) H_z \tag{14}$$

$$\left\{\hat{\mathbf{z}} \times \nabla_T \mu \left[k_z^2 - k_0^2 \mu \boldsymbol{\epsilon}_T\right]^{-1} \hat{\mathbf{z}} \times \nabla_T - \mu\right\} H_z = q_z (\hat{\mathbf{z}} \times \nabla_T) \left[k_z^2 - k_0^2 \mu \boldsymbol{\epsilon}_T\right]^{-1} \nabla_T E_z, \tag{15}$$

where the operators are given by

$$-r^2 \nabla_T \boldsymbol{\epsilon}_T \left[k_z^2 - k_0^2 \mu \boldsymbol{\epsilon}_T\right]^{-1} \nabla_T = \frac{\epsilon_\rho}{q_\rho^2} \left[r\partial_r\right]^2 + \frac{\epsilon_\phi}{q_\phi^2} \partial_\phi^2, \tag{16}$$

$$-r^2 \hat{\mathbf{z}} \times \nabla_T \left[k_z^2 - k_0^2 \mu \boldsymbol{\epsilon}_T\right]^{-1} \hat{\mathbf{z}} \times \nabla_T = \frac{1}{q_\phi^2} \left[r\partial_r\right]^2 + \frac{1}{q_\rho^2} \partial_\phi^2, \tag{17}$$

$$-r^2 \nabla_T \left[k_z^2 - k_0^2 \mu \boldsymbol{\epsilon}_T\right]^{-1} (\hat{\mathbf{z}} \times \nabla_T) = r^2 (\hat{\mathbf{z}} \times \nabla_T) \left[k_z^2 - k_0^2 \mu \boldsymbol{\epsilon}_T\right]^{-1} \nabla_T = \left(\frac{1}{q_\phi^2} - \frac{1}{q_\rho^2}\right) r\partial_r \partial_\phi = \frac{\mu\left(\epsilon_\rho - \epsilon_\phi\right)}{q_\rho^2 q_\phi^2} r\partial_r \partial_\phi. \tag{18}$$

For the Fourier harmonics of the longitudinal components

$$E_z = E_m(r)\, e^{im\phi}, \quad H_z = -iH_m(r)\, e^{im\phi}, \quad \partial_\phi \longrightarrow im, \tag{19}$$

where $m \in \mathbb{Z}$ is the azimuthal number enumerating the harmonics, we derive the following system of equations:

$$\begin{pmatrix} \epsilon_\rho q_\phi^2 \left[r\partial_r\right]^2 - \epsilon_\phi q_\rho^2 m^2 + \epsilon_{zz} q^2 r^2 & m\kappa_z r\partial_r \\ m\kappa_z r\partial_r & \mu q_\rho^2 \left[r\partial_r\right]^2 - \mu q_\phi^2 m^2 + \mu q^2 r^2 \end{pmatrix} \begin{pmatrix} E_m \\ H_m \end{pmatrix} = \mathbf{0}, \tag{20}$$

where $q^2 = q_\rho^2 q_\phi^2$, $\kappa_z = q_z \mu \Delta\epsilon$ and $\Delta\epsilon = \epsilon_\rho - \epsilon_\phi$.

2.2. Boundary Conditions and Dispersion Relations. For the special case of a zero mode with $m = 0$, the solution of the system (20) can be readily found and is given by

$$E_z = E_0(r) = A_0 J_0\left(r_{z\rho} q_\rho r\right), \quad iH_z = H_0(r) = B_0 J_0\left(q_\phi r\right), \quad r_{z\rho}^2 = \frac{\epsilon_{zz}}{\epsilon_\rho}. \tag{21}$$

In general case, we introduce the matrix notations

$$\mathbf{A}(\alpha) = \begin{pmatrix} \epsilon_\rho q_\phi^2 \alpha^2 - \epsilon_\phi q_\rho^2 m^2 & m\kappa_z \alpha \\ m\kappa_z \alpha & \mu q_\rho^2 \alpha^2 - \mu q_\phi^2 m^2 \end{pmatrix}, \quad \mathbf{B} = q^2 \begin{pmatrix} \epsilon_{zz} & 0 \\ 0 & \mu \end{pmatrix} \tag{22}$$

and will search for the solutions of the system (20) that are regular at $r = 0$ (on the waveguide axis) in the form of a power series:

$$\begin{pmatrix} E_{m,\alpha}(r) \\ H_{m,\alpha}(r) \end{pmatrix} = r^\alpha \sum_{n=0}^{\infty} \mathbf{c}_n r^n. \tag{23}$$

Substitution of the expansion (23) into Eq. (20) gives the equation for the coefficient $\mathbf{c}_0$ and the recurrence relations for $\mathbf{c}_n$:

$$\mathbf{A}_0 \mathbf{c}_0 = 0, \quad \mathbf{c}_n = -\mathbf{A}_n^{-1} \mathbf{B} \mathbf{c}_{n-2}, \quad \mathbf{A}_n \equiv \mathbf{A}(\alpha + n). \tag{24}$$

The values of the parameter α can be found from the singularity condition for the matrix $\mathbf{A}_0$:

$$\det \mathbf{A}(\alpha) = n_\rho^2 q^2 \alpha^4 - \alpha^2 m^2 \left(n_\phi^2 q_\rho^4 + n_\rho^2 q_\phi^4 + \kappa_z^2\right) + n_\phi^2 q^2 m^4 = 0, \tag{25}$$

giving two positive values of the parameter $\alpha \in \{\alpha_+, \alpha_-\}$ that define two solutions which are regular at $r = 0$. Note that, similar to the case of Bessel functions of the first kind $J_\nu(x)$, we can use the expression for the determinant of the matrix $\mathbf{A}_n$ (at $\alpha = \alpha_\pm$):

$$\det \mathbf{A}_n = n_\rho^2 q^2 \left[(\alpha + n)^4 - \alpha^4\right] - \left(m\kappa_z\right)^2 \left[(\alpha + n)^2 - \alpha^2\right] \tag{26}$$

to prove convergence of the power series (23), representing an entire function.

The obtained solution can be used not only for analyzing the waveguide regime, but also for describing the light scattering by radially anisotropic scatterers without recourse to the simplifying assumptions such as $E_z = 0$ used in the literature [22, 23].

Now, following [2], we concentrate on the important special case with $\epsilon_\rho = \epsilon_\phi \equiv \epsilon_t$. In this case we have

$$\begin{aligned} E_z &= E_m(r) = A_m J_m(r_{zt} q_t r), \\ iH_z &= H_m(r) = B_m J_m(q_t r), \\ r_{zt}^2 &= \frac{\epsilon_{zz}}{\epsilon_t}, \end{aligned} \tag{27}$$

where $q_t^2 = n_t^2 - q_z^2$.

Outside the waveguide at $r > k_0 R \equiv x$, the solution that exponentially decreases at infinity, $E_z, H_z \propto e^{-r}/\sqrt{r}$, is given by

$$\begin{aligned} E_z &= E_m(r) = a_m K_m(q_c r), \\ iH_z &= H_m(r) = b_m K_m(q_c r), \\ q_c^2 &= q_z^2 - n_c^2 \end{aligned} \tag{28}$$

where $K_m(x)$ is the modified Bessel function [24] and $n_c = \sqrt{\mu_c \epsilon_c}$ is the refractive index of the ambient medium.

From the continuity conditions for the tangential components of the electromagnetic field at the waveguide boundary

$$\begin{aligned} E_z(x+0) &= E_z(x-0), \\ H_z(x+0) &= H_z(x-0), \\ E_\phi(x+0) &= E_\phi(x-0), \\ H_\phi(x+0) &= H_\phi(x-0), \end{aligned} \tag{29}$$

$$x \equiv k_0 R \tag{30}$$

we have

$$\begin{aligned} &\mathbf{C}_m \begin{pmatrix} \alpha_m \\ \beta_m \end{pmatrix} = \mathbf{0}, \\ &\alpha_m = A_m J_m(r_{zt} x_t) = a_m K_m(x_c), \ \beta_m = B_m J_m(x_t) = b_m K_m(x_c), \end{aligned} \tag{31}$$

where $x_t = q_t x$, $x_c = q_c x$ and the matrix $\mathbf{C}_m$ is given by

$$\mathbf{C}_m = \begin{pmatrix} q_z m\left(n_t^2 - n_c^2\right) & \mu q_c^2 R_J^{(m)}(x_t) + \mu_c q_t^2 R_K^{(m)}(x_c) \\ \epsilon_t q_c^2 R_J^{(m)}(r_{zt} x_t) + \epsilon_c q_t^2 R_K^{(m)}(x_c) & q_z m\left(n_t^2 - n_c^2\right) \end{pmatrix}, \tag{32}$$

$$\begin{aligned} R_J^{(m)}(x) &= \frac{x J_m'(x)}{J_m(x)} = m - \frac{x J_{m+1}(x)}{J_m(x)}, \\ R_K^{(m)}(x) &= \frac{x K_m'(x)}{K_m(x)} = m - \frac{x K_{m+1}(x)}{K_m(x)}. \end{aligned} \tag{33}$$

Dispersion relations for the harmonics of the electromagnetic field, linking k_z and $k_0 = \omega/c$, can be deduced from the singularity condition for the matrix (32):

$$\begin{aligned} &\det \mathbf{C}_m(q_z, x) = 0, \\ &n_c^2 \le q_z^2 = \left(\frac{k_z}{k_0}\right)^2 \le n_t^2, \\ &x = k_0 R. \end{aligned} \tag{34}$$

2.3. Numerical Results. We begin our analysis with the case of waveguide modes with the zero azimuthal number: $m = 0$. In this case, the dispersion relations are simplified and reduced to the relations for two types of the waves: TE waves with $E_z = 0$

$$\begin{aligned} &\mu q_c^2 R_J^{(0)}(x_t) = -\mu_c q_t^2 R_K^{(0)}(x_c) \Longrightarrow \\ &\frac{\mu J_1(x_t)}{x_t J_0(x_t)} = -\frac{\mu_c K_1(x_c)}{x_c K_0(x_c)} \end{aligned} \tag{35}$$

and TH waves with $H_z = 0$

$$\begin{aligned} &\epsilon_t q_c^2 R_J^{(0)}(r_{zt} x_t) = -\epsilon_c q_t^2 R_K^{(0)}(x_c) \Longrightarrow \\ &\frac{\epsilon_z J_1(r_{zt} x_t)}{r_{zt} x_t J_0(r_{zt} x_t)} = -\frac{\epsilon_c K_1(x_c)}{x_c K_0(x_c)}. \end{aligned} \tag{36}$$

The roots of Eqs. (35) and (36) are located between the corresponding zeros of the Bessel function J_0 and will be numbered in ascending order by the index l. In our subsequent calculations, we shall use the estimates taken from the paper [11]: the pores of radius R that ranged from 200 nm to 600 nm are filled with the nematic liquid crystal 5CB characterized by the refractive indices $n_e \approx 1.72$ and $n_o \approx 1.5$ ($\mu = 1$), the effective refractive index of the polymer matrix is $n_c \approx 1.57$ ($\mu_c = 1$), and the wavelength of the laser radiation is $\lambda = 632$ nm. Clearly, in this case, we have $2 \approx 1.98 \le k_0 R \le 5.96 \approx 6$.

Figure 1 shows how liquid crystal anisotropy (the value of the longitudinal refractive index n_z) affects the dispersion curves for the waveguide modes TE_{0l} and TH_{0l}. It can be seen that the curves for the TE modes, which are computed for the planar director configuration with the effective refractive index $n_t = n_e = 1.72$, are independent of n_z (see Eq. (35)), whereas the difference between the dispersion curves

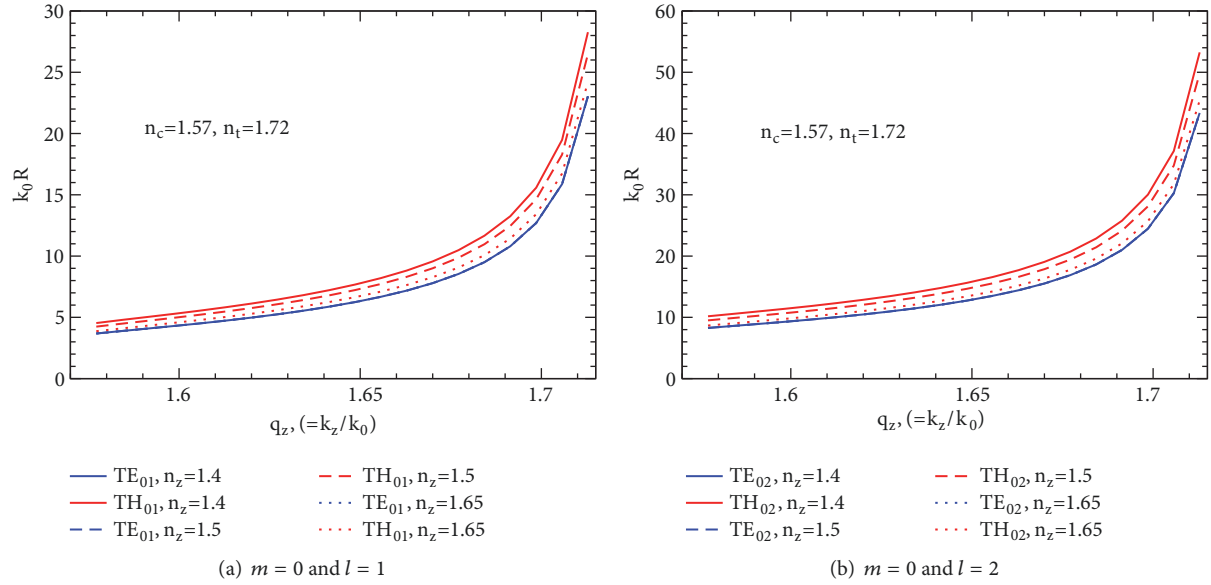

(a) $m = 0$ and $l = 1$ (b) $m = 0$ and $l = 2$

FIGURE 1: Dependence of the dimensionless parameter $k_0R \equiv \omega R/c$ on $q_z = k_z/k_0$ for TE_{ml} ($E_z = 0$) and TH_{ml} ($H_z = 0$) waves with $m = 0$: (a) $l = 1$ and (b) $l = 2$ (index l enumerates the branches of roots in ascending order) at different values of the refractive index n_z.

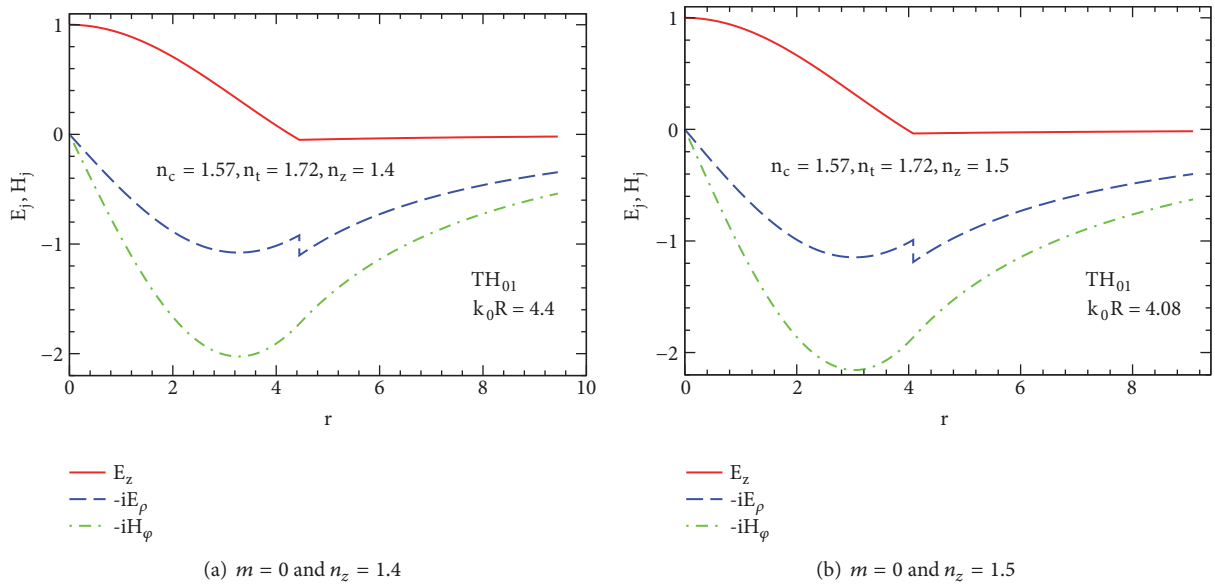

(a) $m = 0$ and $n_z = 1.4$ (b) $m = 0$ and $n_z = 1.5$

FIGURE 2: Electromagnetic field versus the dimensionless radial parameter $r = k_0\rho$ for the mode TH_{01} ($H_z = 0$) at (a) $n_z = 1.4$ and (b) $n_z = 1.5$.

for the TH and TE modes becomes more pronounced as the difference between the refractive indices n_t and n_z increases. The radial distributions of nonvanishing components of the electromagnetic fields for the waveguide modes TH_{01} and TE_{01} are presented in Figures 2 and 3, respectively.

The results illustrating effect of n_z on the hybrid modes ($E_z \neq 0$ and $H_z \neq 0$) with $m = 1$ and $m = 2$ are plotted in Figure 4. It is seen that as compared to the TH modes the curves for the hybrid modes are much less sensitive to variations in n_z. Interestingly, for such modes, similar to the case of TH_{01} and TE_{01} modes, the waveguide regime may occur in the porous films, where $2 \leq k_0R \leq 6$.

When the electric field is applied, the effective refractive indices of the LC (in a typical situation n_t decreases, whereas n_z increases) and the waveguide regime in the porous film can be suppressed. This is obvious if the refractive index n_t, which approaches $n_o < n_c$ as the field increases, becomes less than n_c, so that the condition of total internal reflection appears to be violated. Figure 5 shows the dispersion curves

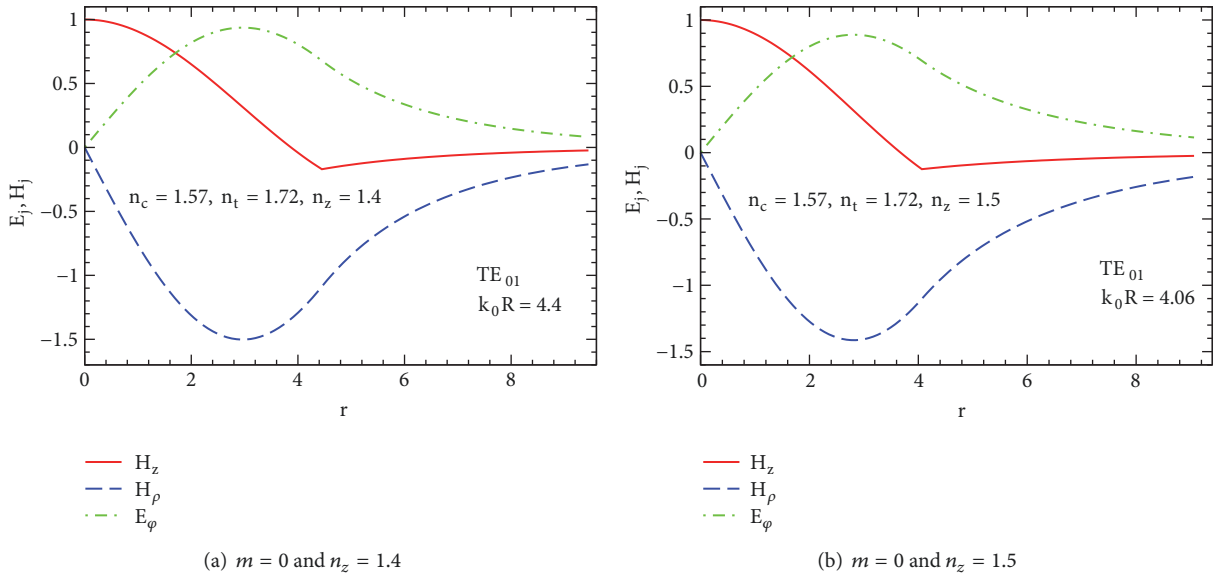

(a) $m = 0$ and $n_z = 1.4$ (b) $m = 0$ and $n_z = 1.5$

FIGURE 3: Electromagnetic field versus the dimensionless radial parameter $r = k_0\rho$ for the mode TE_{01} ($E_z = 0$) at (a) $n_z = 1.4$ and (b) $n_z = 1.5$.

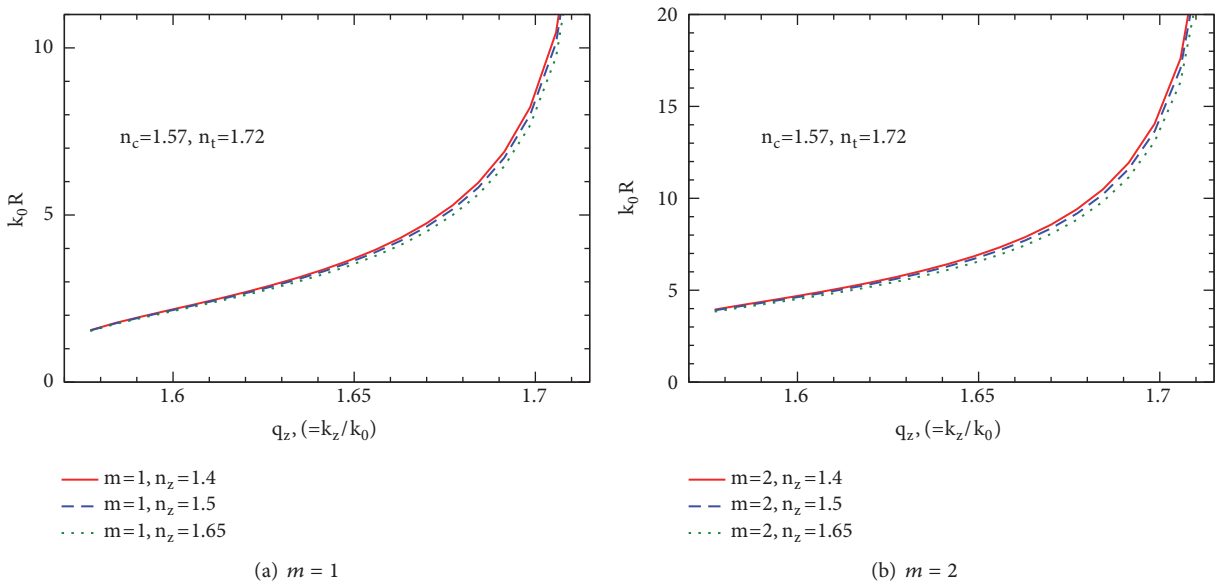

(a) $m = 1$ (b) $m = 2$

FIGURE 4: Dependence of the dimensionless parameter $k_0R \equiv \omega R/c$ on $q_z = k_z/k_0$ for the waves with (a) $m = 1$ and (b) $m = 2$ at different values of the refractive index n_z.

for the case when the configuration distorted by the field is close to axial with $n_z = n_e$, but n_t is still higher than n_c. It is interesting that under these conditions, for a film with $2 \le k_0R \le 6$, the conditions for the waveguide propagation regime are satisfied only for the hybrid mode with $m = 1$.

Radial distributions for the components of the electric and magnetic fields are shown in Figures 6 and 7, respectively. These figures, in particular, demonstrate that the degree of the field localization inside the pore decreases as the director configuration approaches the axial structure.

3. Experiment

3.1. Experimental Procedure. In our experiments, we have used two types of PET films that are characterized by both micron-sized (the diameter is $d = 5\,\mu$m) and submicron-sized ($d = 0.6\,\mu$m) pores without any surfactant treatment. The PET films of thickness $h = 23\,\mu$m were obtained by heavy ion bombarding with subsequent chemical etching. Axes of open-end pores were normal to the surface of the films. The PET films were rinsed two times with ethanol, blown, and then vacuumed to remove a solvent.

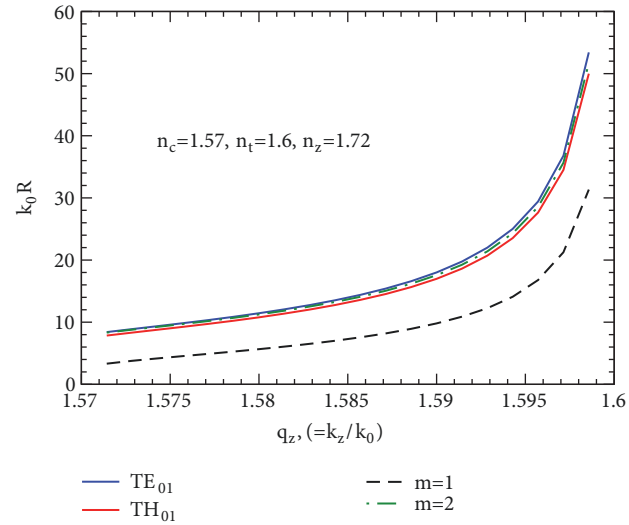

FIGURE 5: Dimensionless parameter $k_0R \equiv \omega R/c$ as a function of $q_z = k_z/k_0$ for the waves with $0 \leq m \leq 2$ at $n_z = 1.72 > n_t = 1.6 \approx n_c$.

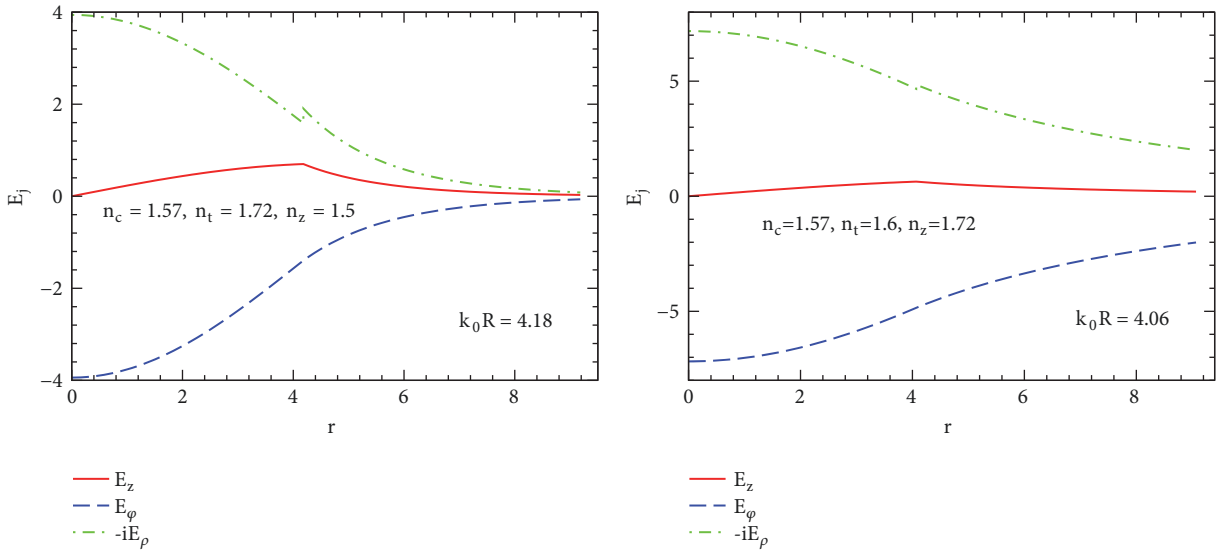

(a) $m = 1$ and $n_z = 1.5$ (b) $m = 1$ and $n_z = 1.72$

FIGURE 6: Components of electromagnetic field as a function of the dimensionless radial parameter $r = k_0\rho$ for the mode with $m = 1$ at (a) $n_z = 1.5$ and (b) $n_z = 1.72$.

The films were filled with nematic liquid crystal (4-n-pentyl-4'-cyanobiphenyl, 5CB) in isotropic phase and then slowly cooled down to room temperature. Afterwards, the films were wiped to remove parasitic LC layers on their surfaces.

Two different cells and experimental set-ups were used for the optical study of light propagation through the PET films filled with 5CB. In the case of the film with submicron pores, we measured the integral intensity of He-Ne laser (the wavelength is $\lambda = 0.633\,\mu$m) beam passed through the PET film. The linearly polarized beam was normally incident on the PET film sandwiched between two glass substrates with ITO electrodes and placed on an optical bench. The intensity of light was measured at fixed angles β between the optical axis of the film and the polarization plane of the beam using the scheme without an analyzer to avoid the birefringence effects.

In the films with micron pores, we studied the optical textures of 5CB within the individual micron-sized pores of the PET film. In this case, the film was stacked between two glass plates. The lower glass plate contained ITO layer with inter-electrode gap of the width g= 50 μm needed to arrange in-plane electric field, applied to the sample. Polarized optical microscopy (POM) with 1000x magnification was used to study optical textures of 5CB in both crossed and parallel polarizers for the LC cell differently oriented with respect to them.

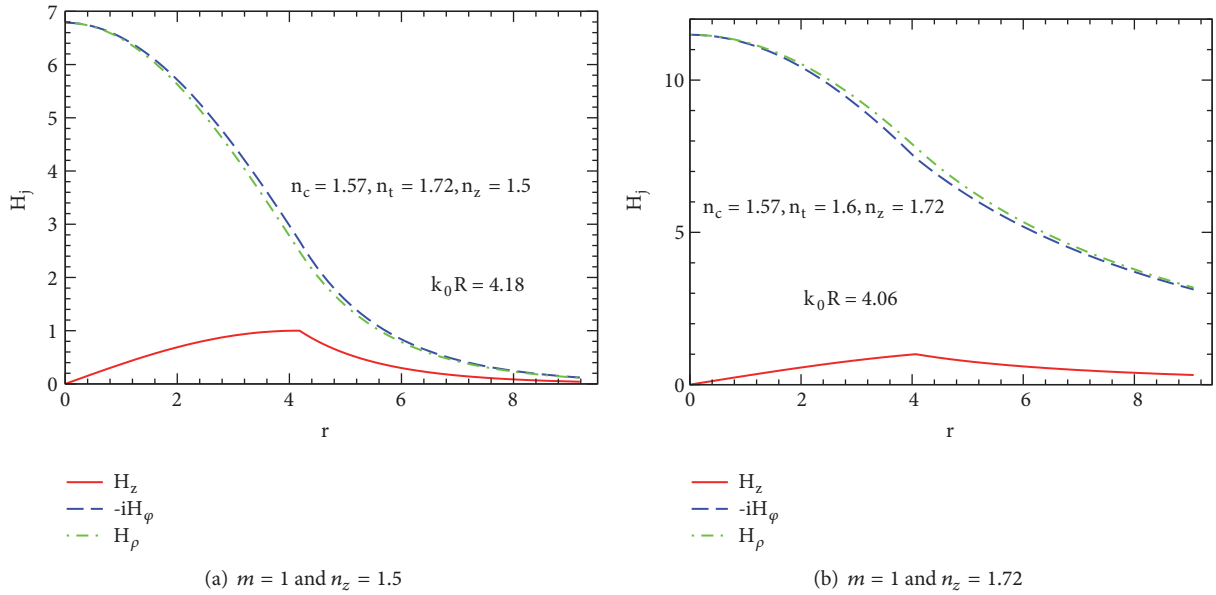

(a) $m = 1$ and $n_z = 1.5$ (b) $m = 1$ and $n_z = 1.72$

FIGURE 7: Components of electromagnetic field as a function of the dimensionless radial parameter $r = k_0\rho$ for the mode with $m = 1$ at (a) $n_z = 1.5$ and (b) $n_z = 1.72$.

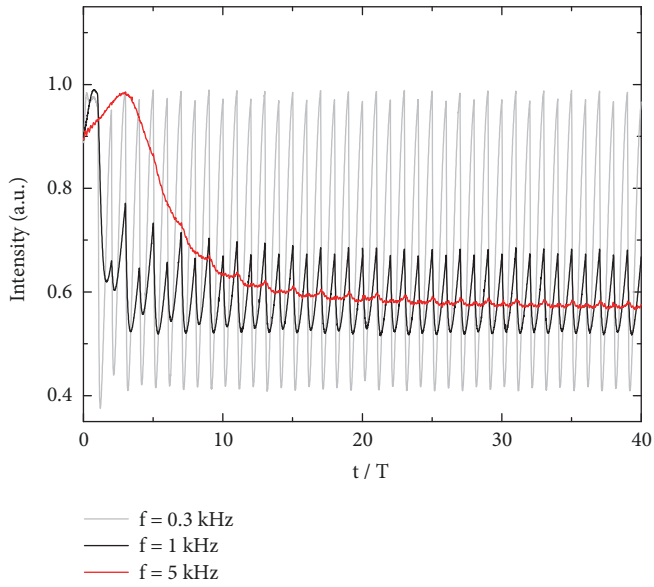

FIGURE 8: The dependence of a light intensity I passed through the PET-5CB film as a function of the dimensionless time parameter t/T at different frequencies $f = 0.3 \ldots 5$ kHz of the applied electric field: $T = 1/2f$; the voltage $U = 170$ V.

3.2. Experimental Results and Discussion. The electrooptical response of the sample at different frequencies of the applied field is shown in Figure 8. At high frequency ($f = 5$ kHz), it looks like a typical response of planar layers of LC with the positive dielectric permittivity anisotropy in crossed polarizers, oriented at 45° with respect to the optical axis. So, the dielectric mechanism of action of electric field on LC, giving rise to overall rotation of the director towards the pore's axis, is responsible for the observed effect.

In particular, the field induced distortions of the initial configuration results in the decrease of the effective anisotropy of LC, introduced by the theoretical model, and disappearance of the waveguide modes, sensitive to this parameter. It leads to decreasing of the light intensity registered in the experiment. In the case of strong electric fields, one can expect the breaking of surface anchoring [2] and formation of the axial LC configuration. This configuration is characterized by the ordinary refractive index which is lower than the indexes of the polymer matrix, so that the waveguide regime appears to be suppressed. The effective value of the electric field strength (of order 1 V/μm) is comparable with the critical values for such orientational transformation

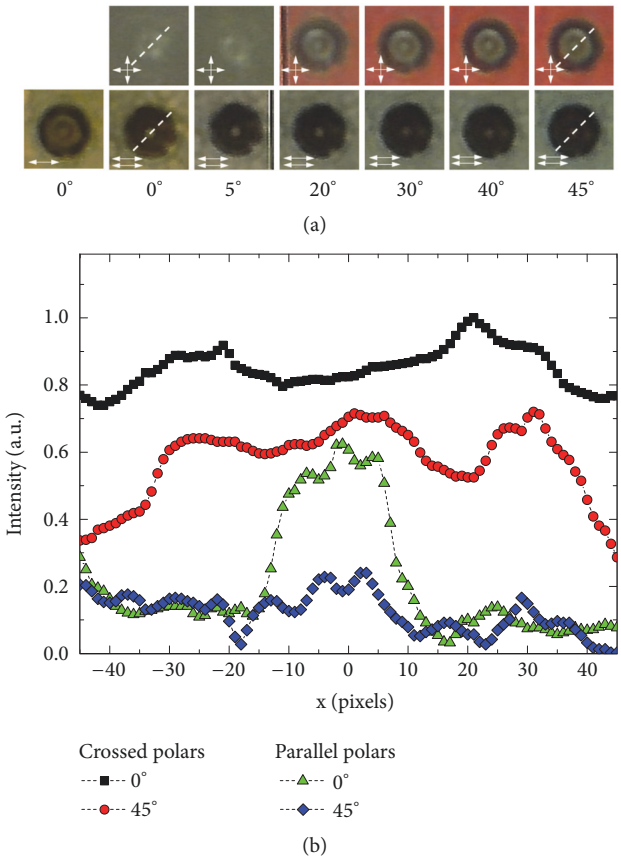

FIGURE 9: (a) Microscopic images of a single pore of the PET film filled with LC and (b) the intensity profiles measured along the dashed lines for the film rotated by different angles with respect to the polarizers.

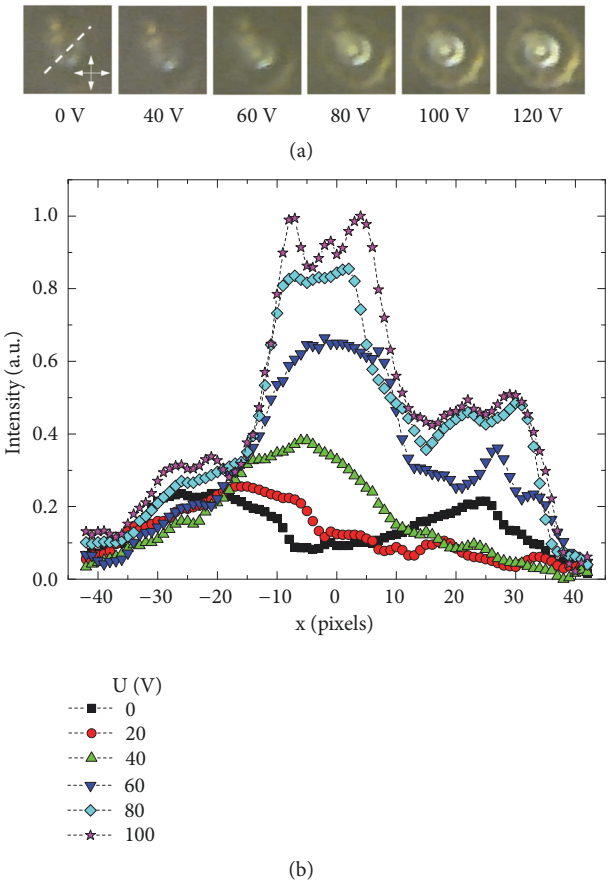

FIGURE 10: (a) Microscopic images of a single pore filled with LC for different values of the applied voltage (the voltage U is ranged from 0 to 120 V and $f = 3$ kHz) and (b) the intensity profiles measured along the dashed line.

obtained via the computer simulation [2] for a nematic mixture E7 with material parameters close to those for 5CB.

So, the breaking of the surface anchoring with corresponding light scattering can be responsible for strong decrease of the light intensity observed in our experiments. It is also important to notice that such type of response is drastically different from the low frequency response shown in Figure 8. This response can be explained by the additional influence of ion's motion [12]. Nevertheless, the strong decrease of the instant values of light intensity, registered in this case, can be also explained by the abovementioned mechanism.

We also directly studied the propagation of light through the single micrometer-sized pores ($d = 5\,\mu$m) of the PET film filled with LC by analyzing the optical textures. Figure 9(a) shows the microscopic images of the PET-LC film differently oriented with respect to the crossed (parallel) polarizers. For the crossed polarizers, the majority of pores reveal the cross-like texture indicating orientation of the director field either along or perpendicular to the dark lines. Such behavior may take place as a result of different director configurations within pores.

In contrast to the case of crossed polarizers, a bright state appears for the film rotated about the normal by 45 degrees. This points to the existence of the symmetry axis for the director configuration, which is typical for both planar (the planar polar configuration) and homeotropic (the axial polar configuration) anchoring. At the same time, the dark-to-bright transition as the film is rotated with respect to the crossed polarizers results in the formation of the ring in the central region of the pores. It should also be noted that the bright spot surrounded by the dark area within the pores was observed in the parallel polarizers (see the lower panel of Figure 9(a)). Usually observation of the dark areas in the parallel polarizers points to the twisting orientational LC structure. Observation of the bright spot surrounded by the dark ring can be explained as a result of waveguide propagation of light in the pore. Since the defectless cross-like figure in crossed polarizers corresponds to the uniform LC structure within the pores, observation of the dark area surrounding the bright spot indicates violation of the propagation of polarization light. In this case, the distribution of brightness (the light intensity as we assume in this study) strongly depends on the polarization state of light (see Figure 9(b)).

The dark-to-bright transition was also caused by the in-plane ac electric field applied to the PET-LC film (see Figure 10(a)). In this case, the electric field induced the twist

torque that reorients the bulk director of LC within the pores in the plane of the PET film. It produces the rotation of the symmetry axis of the LC structure along the field lines. Therefore, the symmetry axis of LC configuration twisted from the side of the cell with inter-electrode gap to the glass substrate without ITO that mimics the helicoid LC structure within the pores.

Since the electric coherence length (the length that characterizes the thickness of a boundary layer, with the orientation stabilized by surface in the presence of electric field) decreases with the voltage, it explains the increase in the intensity of light passed through the single pore (see Figure 10(b)).

From the above discussion, we arrive at the conclusion that the waveguide light propagation strongly depends on the orientational LC configuration formed inside the pores and can be effectively controlled by applying either in-plane or out-of-plane electric fields to the PET-LC film.

4. Conclusion

In this paper we have theoretically studied the light propagation in a cylindrical waveguide filled with the material characterized by the biaxial radial optical anisotropy. The analysis of the obtained dispersion relations for the waveguide modes showed that, when the electric field is applied to the porous film, the waveguide propagation regime is possible for the hybrid mode with the azimuthal number $m = 1$, until the total internal reflection condition is violated. We have also presented some experimental results on the waveguide regime of light propagation in polymer PET porous films with micro-sized and submicro-sized pores filled with the nematic liquid crystal 5CB in the presence of electric fields. In particular, we have found that the pronounced decrease of the transmitted light intensity induced by the strong electric field applied along the submicro-sized pore's axis can be explained by the suppression of the propagating waveguide modes resulting from the surface anchoring breaking and the formation of the axial configuration. At the same time, in-plane electric field, applied to the micro-sized pores, results in essential changes of the inhomogeneous light intensity distribution across the pore's cross-section, which can be assigned to the electrically induced twist deformation of the initial director configuration.

The part of our analysis was concerned with the special case where $\epsilon_\rho = \epsilon_\phi \equiv \epsilon_t$. It relies on the assumption that the optical properties of the pores can be described by the effective dielectric tensor averaged over the LC director distribution: $\epsilon_{ij}^{(\mathrm{eff})} = \epsilon_o \delta_{ij} + (\epsilon_e - \epsilon_o)\langle d_i d_j \rangle$. In [2], this approximation was applied to the escaped radial configuration in 5CB cells with the director field of the form $\widehat{\mathbf{d}} = \cos\chi(\rho)\widehat{\mathbf{e}}_\rho + \sin\chi(\rho)\widehat{\mathbf{z}}$ characterized by the angle $\chi(\rho)$. In this case, the principle values of the effective dielectric tensor are $\epsilon_t = \epsilon_o + (\epsilon_e - \epsilon_o)\langle\cos^2\chi\rangle/2$ and $\epsilon_{zz} = \epsilon_o + (\epsilon_e - \epsilon_o)\langle\sin^2\chi\rangle$, where $\langle\cos^2\chi\rangle = 2R^{-2}\int_0^R \cos^2\chi(\rho)\rho\mathrm{d}\rho$.

Heuristically, validity of the above approximation can be justified using the condition of weakly inhomogeneous anisotropy that can be written in the form

$$k_0 R\delta n < 1, \tag{37}$$

where $\delta n = \max|\sqrt{\boldsymbol{\epsilon}_{\mathrm{eff}}} - \sqrt{\boldsymbol{\epsilon}}|$ is the refractive index variation characterizing the difference between the effective and local values of the refractive indices. For the escaped radial configuration in the 5CB cell without applied electric field, it is not difficult to estimate the refractive index variation at about $\delta n \approx 0.1$. In deriving this estimate, we have assumed strong homeotropic anchoring conditions so that $\cos\chi(R)$ is close to unity. Electric field applied across the film and weak anchoring conditions are the factors that may considerably reduce δn. Our results, however, indicate that, for micron-sized pores, the approximation based on the effective dielectric tensor breaks down.

Our concluding remark is that, in addition to the description of the waveguide regime in optically anisotropic cylindrical waveguides, our analytical results can be used to extend the class of exactly solvable problems of the theory of light scattering. Further investigations suggest solving the problem of light transmission for optically anisotropic porous films that, in particular, will require a more sophisticated analysis using the methods of the effective medium theory.

Data Availability

The data used to support the findings of this study are included within the article.

Conflicts of Interest

The authors declare that they have no conflicts of interest.

Acknowledgments

The authors acknowledge financial support from the Ministry of Education and Science of the Russian Federation (Project No. RFMEFI58316X0058).

References

[1] A. Corella-Madueño and J. A. Reyes, "Electrically controlled liquid crystal fiber," *Optics Communications*, vol. 264, no. 1, pp. 148–155, 2006.

[2] V. Tkachenko, A. A. Dyomin, G. V. Tkachenko, G. Abbate, and I. A. Sukhoivanov, "Electrical reorientation of liquid crystal molecules inside cylindrical pores for photonic device applications," *Journal of Optics A: Pure and Applied Optics*, vol. 10, no. 5, Article ID 055301, 2008.

[3] M. Wahle and H.-S. Kitzerow, "Liquid crystal assisted optical fibres," *Optics Express*, vol. 22, no. 1, pp. 262–273, 2014.

[4] C. Markos, J. C. Travers, A. Abdolvand, B. J. Eggleton, and O. Bang, "Hybrid photonic-crystal fiber," *Reviews of Modern Physics*, vol. 89, no. 4, Article ID 045003, 2017.

[5] J. Beeckman, K. Neyts, and P. J. M. Vanbrabant, "Liquid-crystal photonic applications," *Optical Engineering*, vol. 50, no. 8, Article ID 081202, 2011.

[6] S. V. Pasechnik, V. G. Chigrinov, and D. V. Shmeliova, *Liquid Crystals: Viscous and Elastic Properties*, Wiley-VCH, Berlin, Germany, 2009.

[7] R. J. Carlton, J. T. Hunter, D. S. Miller et al., "Chemical and biological sensing using liquid crystals," *Liquid Crystals Reviews*, vol. 1, no. 1, pp. 29–51, 2013.

[8] R.-P. Pan, C.-Y. Chen, T.-R. Tsai, and C.-L. Pan, "Terahertz phase shifter with nematic liquid crystal in a magnetic field," *Molecular Crystals and Liquid Crystals*, vol. 421, pp. 157–164, 2004.

[9] T. T. Larsen, A. Bjarklev, D. S. Hermann, and J. Broeng, "Optical devices based on liquid crystal photonic bandgap fibres," *Optics Express*, vol. 11, no. 20, pp. 2589–2596, 2003.

[10] D. Semerenko, D. Shmeliova, S. Pasechnik, A. Murauskii, V. Tsvetkov, and V. Chigrinov, "Optically controlled transmission of porous polyethylene terephthalate films filled with nematic liquid crystal," *Optics Letters*, vol. 35, no. 13, pp. 2155–2157, 2010.

[11] A. Chopik, S. Pasechnik, D. Semerenko et al., "Electro-optical effects in porous PET films filled with liquid crystal: New possibilities for fiber optics and THZ applications," *Optics Letters*, vol. 39, no. 6, pp. 1453–1456, 2014.

[12] S. V. Pasechnik, D. V. Shmeliova, A. P. Chopik, D. A. Semerenko, S. S. Kharlamov, and A. V. Dubtsov, "Electrically controlled porous polymer films filled with liquid crystals: New possibilities for photonics and THz applications," in *Proceedings of the 2016 International Conference Days on Diffraction, DD 2016*, pp. 314–318, Russia, July 2016.

[13] H. Lin and P. Palffy-Muhoray, "TE and TM modes in a cylindrical liquid-crystal waveguide," *Optics Letters*, vol. 17, no. 10, pp. 722–724, 1992.

[14] J. A. Reyes and R. F. Rodríguez, "Flow dissipation effects in a nonlinear nematic fiber," *Physical Review E: Statistical, Nonlinear, and Soft Matter Physics*, vol. 65, no. 5, 2002.

[15] R. F. Rodríguez, J. A. Reyes, A. Espinosa-Cerón, J. Fujioka, and B. A. Malomed, "Standard and embedded solitons in nematic optical fibers," *Physical Review E: Statistical, Nonlinear, and Soft Matter Physics*, vol. 68, no. 3, Article ID 036606, 2003.

[16] A. Corella-Madueño and J. Adrián Reyes, "Hydrodynamically controlled optical propagation in a nematic fiber," *Physica B: Condensed Matter*, vol. 403, no. 10-11, pp. 1949–1955, 2008.

[17] D. W. Allender, G. P. Crawford, and J. W. Doane, "Determination of the liquid-crystal surface elastic constant K24," *Physical Review Letters*, vol. 67, no. 11, pp. 1442–1445, 1991.

[18] G. P. Crawford, R. Ondris-Crawford, S. Žumer, and J. W. Doane, "Anchoring and orientational wetting transitions of confined liquid crystals," *Physical Review Letters*, vol. 70, no. 12, pp. 1838–1841, 1993.

[19] S. Kralj and S. Žumer, "The stability diagram of a nematic liquid crystal confined to a cylindrical cavity," *Liquid Crystals*, vol. 15, no. 4, pp. 521–527, 1993.

[20] A. D. Kiselev and V. Y. Reshetnyak, "Stability of the axial director configuration in nematic liquid crystals confined in a cylindrical cavity and the surface-like elastic constant problem," *Journal of Experimental and Theoretical Physics*, vol. 107, pp. 1552–1562, 1995.

[21] A. D. Kiselev and V. Y. Reshetnyak, "Surface elastic constant problems for nlc confined to cylindrical cavity: stability of axial configuration," *Molecular Crystals and Liquid Crystals Science and Technology. Section A. Molecular Crystals and Liquid Crystals*, vol. 265, no. 1, pp. 527–540, 1995.

[22] Y. W. Jin, D. L. Gao, and L. Gao, "Plasmonic resonant light scattering by a cylinder with radial anisotropy," *Progress in Electromagnetics Research*, vol. 106, pp. 335–347, 2010.

[23] H. L. Chen and L. Gao, "Anomalous electromagnetic scattering from radially anisotropic nanowires," *Physical Review A: Atomic, Molecular and Optical Physics*, vol. 86, no. 3, Article ID 033825, 2012.

[24] M. Abramowitz and I. A. Stegun, *Handbook of Mathematical Functions, with Formulas, Graphs, and Mathematical Tables*, Dover, New York, NY, USA, 1972.